2012

Frequency-dependent Transient Response of an Oscillating Electrically Actuated Droplet

S. Dash
Purdue University

N. Kumari

S V. Garimella
Purdue University, sureshg@purdue.edu

Dash, S.; Kumari, N.; and Garimella, S V., "Frequency-dependent Transient Response of an Oscillating Electrically Actuated Droplet" (2012). *CTRC Research Publications.* Paper 178.
http://dx.doi.org/10.1088/0960-1317/22/7/075004

Frequency-dependent transient response of an oscillating electrically actuated droplet

S Dash, N Kumari and S V Garimella[1]

Cooling Technologies Research Center, an NSF IUCRC
School of Mechanical Engineering and Birck Nanotechnology Center
Purdue University
West Lafayette, IN 47907-2088
USA

Abstract

The transient response of a millimeter-sized sessile droplet under electrical actuation is experimentally investigated. Under DC actuation, the droplet spreading rate increases as the applied voltage is increased due to the higher electrical forces induced. At sufficiently high DC voltages, competition between the electrical actuation force, droplet inertia, the retarding surface tension force and contact line friction leads to droplet oscillation. The time scale for the droplet to attain its maximum wetted diameter during step actuation is analyzed. Systematic experiments are conducted over a frequency range of 5 – 200 Hz and actuation voltages of 40 – 80 V_{rms} to determine the dependence of droplet oscillation on these parameters. The response of the droplet to different actuation frequencies and voltages is determined in terms of its contact angle and contact radius variation. The frequency of the driving force (equal to twice the frequency of the applied electrical signal) determines the mode of oscillation of the droplet which, together with its resonance characteristics, governs whether the droplet contact angle and contact radius vary in phase or out of phase with each other. In addition to the primary frequency response at the electrical forcing frequency, the droplet oscillation exhibits sub-harmonic oscillation at half the forcing frequency that is attributed to the parametric nature of the electrical force acting at the triple contact line of the droplet.

Keywords: dynamic contact angle, electrowetting, characteristic time scale, droplet oscillation, resonance, alternating current, sub-harmonic oscillation

[1] Corresponding author email: sureshg@purdue.edu

1. Introduction

Microscale manipulation of droplets by electrical actuation has significant applications in the areas of microfluidics and lab-on-chip devices. Electrowetting-based surface energy control for the actuation of droplets has received significant recent attention because of its lack of moving parts, low power consumption and amenability to integration with microelectronics packaging [1]. Droplet transport, breakup and merging using electrowetting-based actuation have been demonstrated [2-6]. Other key applications that exploit enhanced control of droplet morphology include electrowetting-based optics [7] and liquid displays [8]. Electrowetting (EW) also has application in altering the wetting characteristics of a surface [9-11]. The use of EW in conjunction with changes in surface morphology provides enhanced control of droplet wetting states. The relative stabilities of the Cassie and the Wenzel states on rough surfaces may be manipulated through EW [10,11].

Electrowetting on a dielectric (EWOD) refers to electrowetting on a conducting surface separated from the droplet by an insulating layer, either using AC or DC actuation voltages [1]. The steady-state contact angle of a droplet under DC actuation has been well studied and has been shown to follow Lippmann's equation [1] at lower voltages. Saturation of the contact angle occurs when the applied voltage exceeds a certain value depending on the liquid and dielectric properties [12,13]. Within the working range of actuation voltage, DC electrowetting has been employed in the design of optical displays [14]. Most of the available literature on DC EW has targeted prediction of the steady-state contact angle, while the transient response of the droplet is less well understood. Detailed analysis of the transient response of the droplet under DC actuation is necessary for regulating the response time of EW-based devices. In recent studies, the unsteady motion of a sessile droplet under DC actuation has been reported in terms of the contact radius [15,16].

Electrowetting using AC actuation voltages has also drawn attention [17-19]. The main advantages of using AC voltages over DC include reduction of the chemical reactions in the droplet [4] and decrease in the contact-angle hysteresis [20]. Kumar *et al*. [18] studied the contact angle variation of aqueous salt droplets under an AC voltage. The flow field generated during droplet oscillation under actuation at low AC frequencies can be utilized for enhancing the mixing in a droplet. Mugele *et al*. [21] studied the frequency dependence of the internal flow field in a droplet using tracer particle tracking. Paik *et al*. [22] studied the mixing caused by droplet motion between parallel plates, while Miraghaie *et al*.[23] focused on the shape oscillations to study the internal mixing pattern. Mixing inside a droplet can also be effected by changing the droplet morphology [24]: the droplet is initially in contact with a top electrode when not actuated and detaches from this electrode when actuated. Upon detachment, the droplet is no longer actuated and returns to its original shape at which time it touches the top electrode again. Repetition of this cycle can cause continuous droplet oscillation. Recently, Sen and Kim [16] reported contact angle and radius variations at lower AC frequencies but the experiments were performed for a single actuation voltage. Ko *et al.*[25] used particle image velocimetry to visualize the flow field inside a conducting droplet oscillating under the influence of an AC voltage and attributed the flow at low frequencies to the oscillation of the contact line.

The present work investigates the transient nature of the step response of droplets as well as the important characteristics of the frequency response of the droplet over a range of applied voltages. The first set of experiments maps out the transient response of a millimeter-sized sessile droplet under DC actuation. The response of the droplet, in terms of contact angle (CA) and contact radius (CR) measurements, before it attains a steady-state profile is studied and the characteristic time scale of a droplet during step response is analyzed. Droplet dynamics under low-frequency AC actuation are then investigated in detail in terms of the time-varying CR and

CA with the root-mean-square voltage (V_{rms}) varying from 40 V to 80 V and frequencies ranging from 5 Hz to 200 Hz. The characteristics of the droplet behavior upon contact angle saturation are discussed. The experimental observations map out the different modes of oscillation and also identify the distinct droplet dynamics corresponding to each intermediate frequency regime between two consecutive oscillation modes. The principal as well as the sub-harmonic frequency response of the droplet are identified. The sub-harmonic response is explained in terms of the parametric electrowetting force that governs the droplet oscillation.

2. Experimental setup

A schematic diagram of the experimental setup used for droplet actuation and data acquisition is shown in Figure 1. A highly conducting silicon wafer with a 1 µm thick thermally grown oxide layer was utilized as the substrate. The substrate was spin-coated with a 1% Teflon solution (DuPont) to impart hydrophobicity. An aluminum wire of 125 μm diameter is inserted into the droplet from the top as shown in Figure 1. A voltage difference applied between the silicon wafer and this wire actuates the droplet. De-ionized (DI) water droplets of volume 5 ± 0.1 µl are used in all the experiments. The initial contact angle and the contact radius of the droplet under no electrical actuation are 119° ± 2° and 0.97 ± 0.03 mm, respectively. The gravitational effects on the droplet shape are negligible as the Bond number (*Bo*, the ratio of the gravitational and surface tension forces) is approximately 0.17 and hence the droplet can be assumed to be a spherical cap.

The DC voltage for droplet actuation was provided using a high voltage DC power supply (Kepco BHK 2000- 0.1MG), while the AC voltage was supplied by a variable-frequency signal generator (Tektronix AFG 3022) and a voltage amplifier (Piezo Amplifier EPA-104, Piezo Systems Inc.). The droplet response to the applied actuation was recorded at 1000-2000 fps using a high speed camera (Photron 1024 PCI). All the images were processed using an in-house MATLAB[26] program to determine the dynamic contact angle and interfacial contact radius. The code includes an algorithm to determine the edge of the droplet. The intersection of the droplet image with the corresponding reflected image is used to define the point of contact. A second-order polynomial fit to the detected edge near the contact point gives the best estimate of the droplet profile near the contact. The derivative of the tangent to the curve at the contact point is subsequently used to determine the contact angle. The reported contact angle is the average of the right and the left contact angles. The pixel resolution is 10 microns per pixel. The experimental uncertainties in the measured contact angle and contact radius arising from the imaging and image processing are approximately ± 2° and ± 0.03 mm, respectively. Each experiment was repeated three times, and the variation in measurements was found to be within experimental uncertainty; results from representative cases are presented in the following section. Liquid loss due to evaporation is negligible since the time period of each experiment is on the order of milliseconds.

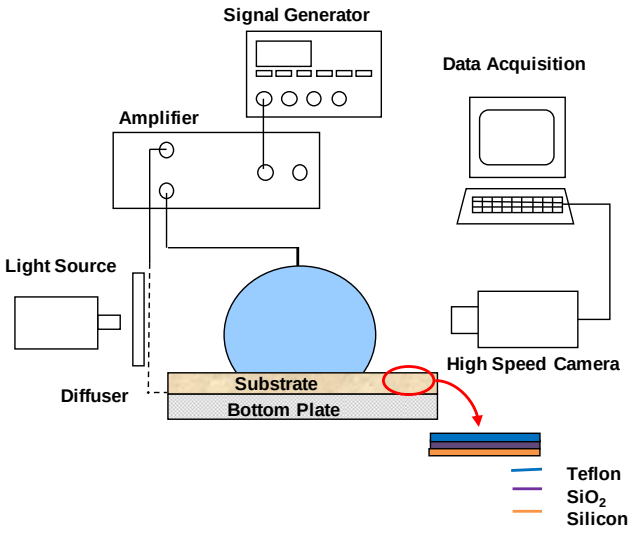

Figure 1. Schematic diagram of the experimental setup.

3. Results and discussion

3.1. DC Actuation

The transient step response of a sessile droplet under DC voltage actuation is studied in the first set of experiments. DC voltages in the range of 40 V to 120 V (in increments of 10 V) are applied to the droplet. The measured steady-state contact angle θ at each voltage is lower than Young's contact angle θ_Y as predicted by Lippmann's equation

$$\cos\theta = \cos\theta_Y + \frac{1}{2\gamma} c V^2 \qquad (1)$$

where V is the applied actuation voltage, γ is the surface tension of the liquid (0.072 N/m for water), and $c = \frac{\varepsilon_0 \varepsilon_r}{d}$ is the capacitance of the dielectric layer, with ε_0 being the vacuum permittivity, ε_r the permittivity constant of the dielectric layer (3.9 for the oxide layer), and d the dielectric thickness (1 μm in the present work). Equation 1 can be written as $\cos\theta = \cos\theta_Y + \left(\frac{V}{V_L}\right)^2$, in which V_L refers to the voltage up to which the Lippmann equation can be used to predict the steady-state droplet contact angle during electrowetting. V_L is defined as $\sqrt{\frac{2\gamma}{c}}$ and is the characteristic voltage scale [24], equal to 65 V for the given experimental conditions. Equation 1 does not apply to the transient variation of droplet contact angle (prior to its attaining a steady shape).

A quantitative comparison of the different dissipation forces involved in electrowetting by Ren *et al.*[27] determined that the contact line friction contributes the dominant dissipative effect. The transient response of the droplet can be modeled in terms of the major horizontal forces acting on the contact line, i.e., surface tension forces, electrowetting force and contact line friction. A simplified mathematical model to understand the transient radial motion of the droplet contact line was developed by Annapragada *et al.*[28]. The droplet transport equation is obtained

by equating the rate of change of momentum per unit length to the sum of all the forces acting at the contact line per unit length.

Figure 2a and Figure 2b show the transient step response of droplet contact angle and contact radius (normalized with respect to the initial contact radius), respectively. The normalized contact radii are used to provide the relative magnitude of droplet spreading with respect to the initial contact radius. At each of the actuation voltages, the contact angle decreases to a steady-state value that depends on the applied DC voltage; the contact radius correspondingly increases during the transient period. The steady-state contact angle decreases as the applied voltage is increased to 80 V, beyond which it saturates. The average steady-state contact angles corresponding to 80 V, 100 V and 120 V are 72.4 ± 0.6°, 73.2 ± 0.3°, and 71.2 ± 1.2°, respectively. Thus the average saturated contact angle of the droplet is 72.2° ± 1.2°. The contact radius has a similar trend, with the steady-state droplet radius reaching approximately 1.54 ± 0.03 mm at voltages higher than or equal to 80 V. The time taken for the droplet to attain a steady shape is approximately 35 ms and varies somewhat depending upon the magnitude of actuation voltage.

An interesting phenomenon of droplet oscillation is observed at high DC voltages. Figure 2b shows that the contact radius increases monotonically to 1.1 mm and 1.4 mm, respectively, at the lower actuation voltages of 40 and 60 V; however, at actuation voltages of 80 V and higher, the contact radius overshoots its equilibrium wetted radius due to higher inertia and induces oscillation in the contact radius and contact angle. Droplet shapes at the actuation voltage of 100 V at different time instances are included in Figure 2b to illustrate this oscillation. For this case, the droplet displays a maximum contact radius of 1.58 mm at t = 9 ms and then recoils to a smaller radius of 1.44 mm at t = 13 ms. The contact line oscillation continues until the droplet attains its equilibrium contact radius of 1.5 mm at t = 25 ms. Similar observations have been made by Oh *et al*. [15] and Sen *et al*.[16]. Independent of the applied voltage, the droplet takes 8 to 9 ms to attain a maximum contact radius, which we define as the characteristic time scale (τ).

The dependence of the characteristic time scale (τ) on the governing parameters –liquid surface tension (γ), liquid density (ρ), droplet radius (R), coefficient of contact line friction (ξ), contact line velocity (v_{CL}), and applied electrical force (Fe) – is determined using the Buckingham Pi theorem with γ, R, ρ as the recurring variables. The resulting nondimensional terms are $\left(\frac{\gamma}{\rho R^3}\right)^{1/2}\tau$, $\left(\frac{1}{\gamma\rho R}\right)^{1/2}\xi$, $\left(\frac{\rho R}{\gamma}\right)^{1/2}v_{CL}$, $\left(\frac{1}{\gamma R}\right)F_e$. After minor rearrangements, the time scale can be represented as a product of $\left(\frac{\rho R^3}{\gamma}\right)^{1/2}$ and a function of the ratios of electrical force and contact line friction with respect to surface tension as: $\tau = \left(\frac{\rho R^3}{\gamma}\right)^{1/2} f\left(\frac{F_e}{\gamma R}, \frac{\xi v_{CL}}{\gamma}\right)$, where F_e/R is the electrical force per unit length and ξv_{CL} is the contact line friction per unit length. The contact line velocity (v_{CL}) increases with increasing actuation voltage (Figure 2). Since the actuation force and the friction force act against each other, it can be assumed that the effect of increased voltage is nullified due the increased friction resulting in $f\left(\frac{F_e}{\gamma R}, \frac{\xi v_{CL}}{\gamma}\right)$ to be more or less a constant. This explains the observed voltage independence of the time scale. A constant

prefactor multiplied with $\left(\frac{\rho R^3}{\gamma}\right)^{1/2}$ describes the experimentally observed time scale for maximum wetted diameter reasonably well. The characteristic time (τ) of the droplet under the present experimental conditions is ~ 9 ms, from which the constant of proportionality is deduced to be ~ 2.4. Thus the characteristic time constant can be written as $2.4\left(\frac{\rho R^3}{\gamma}\right)^{1/2}$. It is interesting to note here the similarity in the expression of this characteristic time scale and the contact time of the droplet impinged on a surface. Richard *et al*. [29] used a scaling analysis between kinetic energy per unit volume of droplet and pressure gradient to study the contact time when a droplet is impinged on a surface and determined the time scale to be independent of its velocity. The time scale was determined to be proportional to $\left(\frac{\rho R^3}{\gamma}\right)^{1/2}$ as well and was independent of the velocity of impingement.

At voltages lower than 60 V (a value that agrees well with the predicted characteristic voltage of 65 V), the electrical actuation force quasi-statically balances the net contact line friction and surface tension, whereas at higher voltages (> 60 V), the higher inertia causes the contact line to overshoot its equilibrium position and undergo damped oscillation under the action of contact line friction. While the contact radius is essentially pinned after one cycle of oscillation, the contact angle continues to oscillate for a longer period as seen in Figure 2a. This can be explained in terms of the two different damping mechanisms namely the contact line friction and viscous dissipation. The contact radius oscillation is damped significantly by the contact line friction, accompanied by a dampening of the contact angle oscillation. The internal flow generated within the droplet due to motion of the contact line and capillary waves on the surface of the droplet takes a much longer time to reach a steady state due to the low viscous dissipation in water resulting in under-damped oscillations of the contact angle and height of the droplet even when the contact radius is pinned. The viscous dissipation is extremely low in comparison to the contact line friction and the ratio is given as $\frac{\xi}{\mu_{water}} = \frac{0.4\,N.s.m^{-2}}{0.001N.s.m^{-2}} = 400$, where ξ is the coefficient of friction; ξ = 0.4 Ns/m^2 is based on the experimental data for the water/Teflon combination from Wang and Jones [30]. This value was also used by Annapragada *et al.*[28] for numerical modeling of droplet dynamics during DC actuation and gave excellent agreement with the present experimental results. The effect of both contact line friction and viscous dissipation in overall dampening as well as suppression of contact angle oscillation due to hysteresis effects explains the time scale for contact angle oscillation not being 400 times greater than the time scale over which the contact radius oscillates before attaining a constant value. The time required to attain the steady-state droplet profile depends on the extent of contact line oscillation which varies with the applied voltage; for example the contact angle oscillation continues for a longer period when actuation voltage is greater than 60 V.

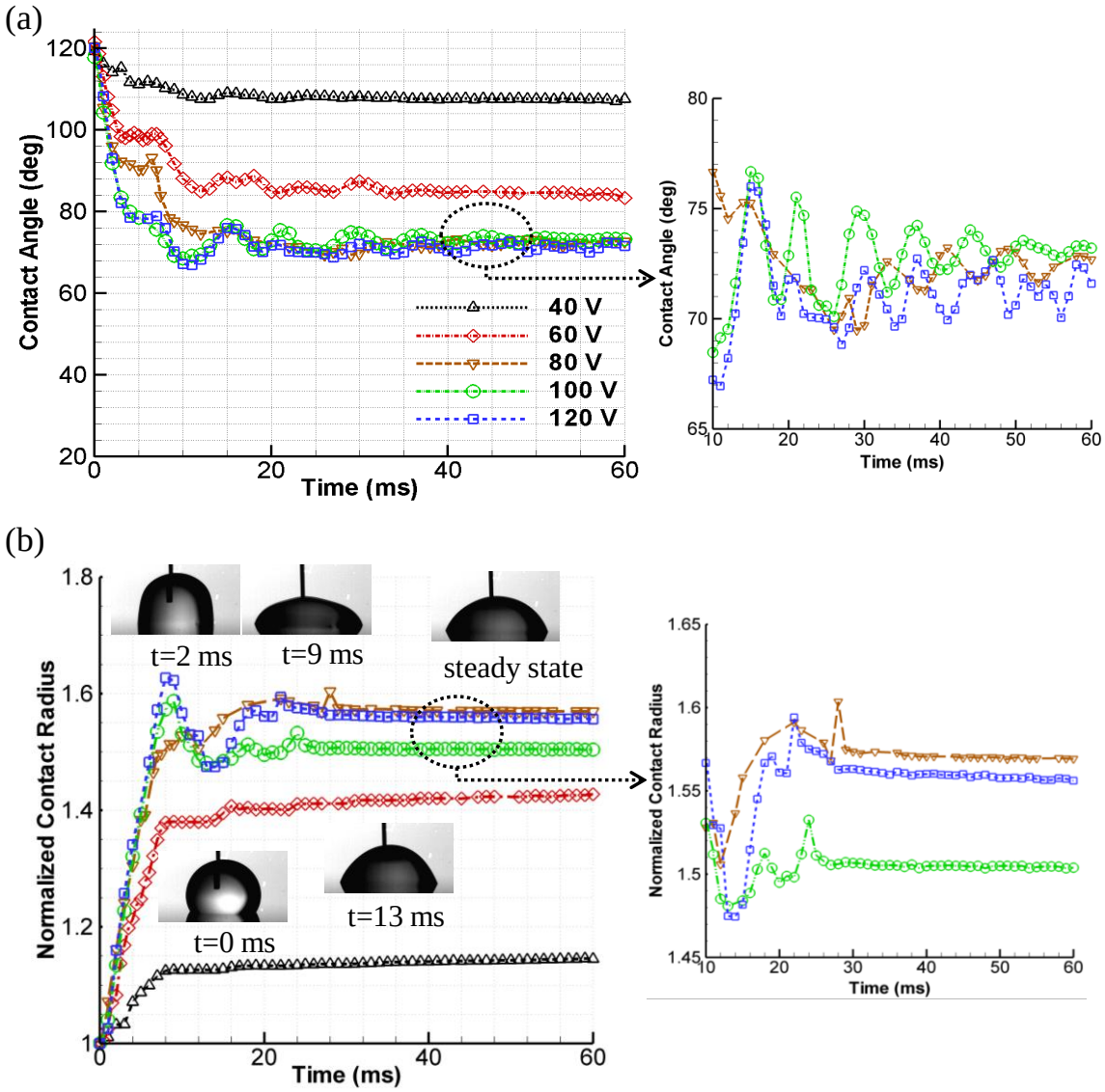

Figure 2. (a) Transient contact angle, and (b) transient contact radius of the droplet illustrating the step response. The droplet images show its response corresponding to the actuation voltage of 100 V. The insets on the right show the zoomed-in data points for actuation voltages of 80 V and greater, at which contact angle saturation occurs.

3.2. AC Actuation

3.2.1 Contact angle and contact radius

Droplet oscillation at sinusoidal AC actuation voltages of 40, 60, and 80 V_{rms} is now explored to determine the combined effects of frequency and applied voltage. The range of frequency of the electrical signal used for the experiments is such that the droplet is able to respond to the electrical force acting at the triple contact line (TCL). The frequency is varied from 5 Hz to 200 Hz in steps of 5 Hz. Results are presented here at representative frequencies of 5, 20, 60, 80, and 120 Hz which reveal the characteristic droplet behavior in the frequency range.

Figure 3a and Figure 3b show the time variation of contact angle and normalized contact radius, respectively, for the three actuation voltages at a frequency of 5 Hz. Results are shown after the first half cycle of droplet oscillation to omit uncertainties involved during the initiation of droplet motion. The symbols show the experimental data and the dashed lines show Fourier-series based curve-fits to the data. At the low frequency (5 Hz), the droplet follows the sinusoidal signal well as the characteristic time scale (9 ms) is much smaller than the time period of the applied electrical force (100 ms). As the electrical forces are proportional to the square of the applied voltage, one cycle of applied signal produces two cycles of droplet oscillation. For the case of 40 V_{rms} the contact angle variation has a sinusoidal shape with a minimum contact angle of 84^0 (Figure 3a). This lower contact angle compared to the measured value of 107^0 for 40 V DC actuation (as seen in Figure 2a) is due to the higher peak voltage of 56 V in the AC signal. As the actuation voltage is increased to 60 V_{rms}, the contact angle is seen to saturate at approximately 70^0 when the instantaneous voltage exceeds 80 V (between 240 ms and 260 ms in Figure 3b). The contact angle saturation occurs at a higher actuation voltage compared to the case of DC actuation (70 V). The saturation effect is more prominent at the higher voltage of 80 V_{rms} (Figure 3b) between the instantaneous values of 80 V and 113 V (corresponding to the time interval from 225 ms to 275 ms). During this period, the CR and CA remain relatively unchanged with time. The main difference in the characteristics of the contact line of the droplet at the 60 V_{rms} and 80 V_{rms} actuation voltages is the velocity at which the droplet reaches its maximum contact radius as derived from the slope of the graph as the droplet reaches the maximum wetted radius (Figure 3b). The measured droplet contact radii for the three cases follow similar trends as the contact angles, as shown in Figure 3b. The contact radius is in phase with the contact angle, i.e., the contact radius increases with a decrease in contact angle. The insets in Figure 3b show the droplet shapes at 150 ms for all three actuation voltages; this time instant corresponds to the maximum spreading.

The non-dimensional contact radius is slightly greater than 1 at the instant of zero actuation due to the effect of contact angle hysteresis. The higher inertia at 60 V_{rms} and 80 V_{rms} as compared to 40 V_{rms} results in a non-dimensional CR equal to 1.01 ± 0.02 as compared to 1.05 ± 0.02 in the latter case (Figure 3b).

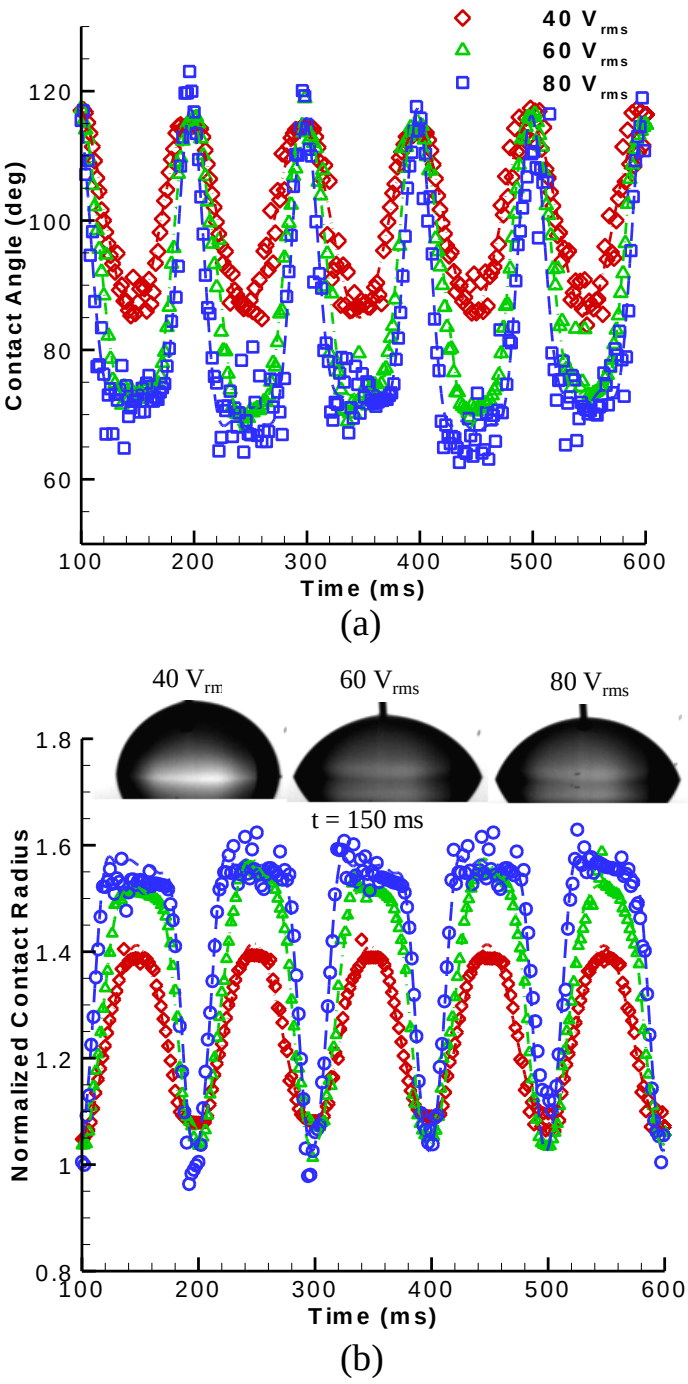

Figure 3. Variation of (a) contact angle, and (b) contact radius for an AC frequency of 5 Hz and V_{rms} = 40 V, 60 V, and 80 V; insets in (b) show the corresponding droplet shapes at 150 ms (symbols – experimental data, dashed line – curve fit).

To understand the effect of actuation frequency on droplet oscillation, the transient contact angles and contact radii for droplet actuation at frequencies of 20, 60, 80, and 120 Hz with AC actuation voltages of 40 V_{rms} and 60 V_{rms} are shown in Figure 4a and Figure 4b, respectively. As before, the plot is shown after the first cycle of the droplet oscillation to omit uncertainties during droplet motion initiation; the symbols show the data as obtained from the experiments, while the

dashed lines are Fourier-series fits. While the droplet oscillations are periodic in nature because of the sinusoidal voltage applied, a number of interesting effects of the actuation frequency are observed. At a constant voltage, the amplitude of oscillation decreases with increasing frequency since the decreased time period of oscillation increases the influence of the characteristic response time. From the step response of the droplet, it is seen that the droplet takes ~ 9 ms to reach its maximum wetted position (Figure 2b). It can be interpreted that the droplet can respond fully to the applied force till a forcing frequency of 111 Hz (with a corresponding signal frequency of 55 Hz). This explains the higher wetted diameters reached at lower actuation frequencies (5 Hz and 20 Hz) as compared to those at frequencies higher than 60 Hz. For example at 120 Hz, the time before the droplet can attain its maximum electrowetted radius is 2.1 ms and is lower than the characteristic time scale. Moreover, oscillation of the droplet is manifested not only as movement of the contact line but also as shape oscillations [32]. Hence the quasi-static response of the contact line to the electrical force as the voltage increases from 0 V to the maximum value in each signal cycle may no longer be assumed. The spherical cap assumption is no longer valid during the droplet oscillation. The plot of the variation of the contact radius with time (Figure 4) suggests an overlap of multiple frequency responses.

At 60 Hz, the contact angle and contact radius are out of phase by a finite angle of 0.75 radians. On the other hand, droplet oscillations at close to resonant frequencies significantly influence the droplet response as will be discussed in the next section. For example, the amplitude of the contact radius oscillation at 120 Hz is seen to be higher than that at 60 Hz (normalized values of 0.08 and 0.06, respectively, for 40 V_{rms}). Moreover, the droplet contact radii and contact angles are in-phase at 80 Hz and out-of-phase by approximately 0.94 radians at 120 Hz, for both 40 V_{rms} and 60 V_{rms}. The contact radius always follows the applied signal; a small time delay is observed at the highest actuation voltage, consistent with the characteristic time constant for complete response. The analysis to follow presents the phase lag between the contact angle and contact radius. It is also noted that the phase lag does not depend on the applied actuation voltage, but only on the actuation frequency; however there is some difference in the behavior of the contact radius at 40 V_{rms} and 60 V_{rms} corresponding to 60 Hz and 80 Hz actuation frequency in terms of the magnitude, but the phase difference remains unchanged. More details regarding the droplet shape dependence on frequency are discussed in the next section.

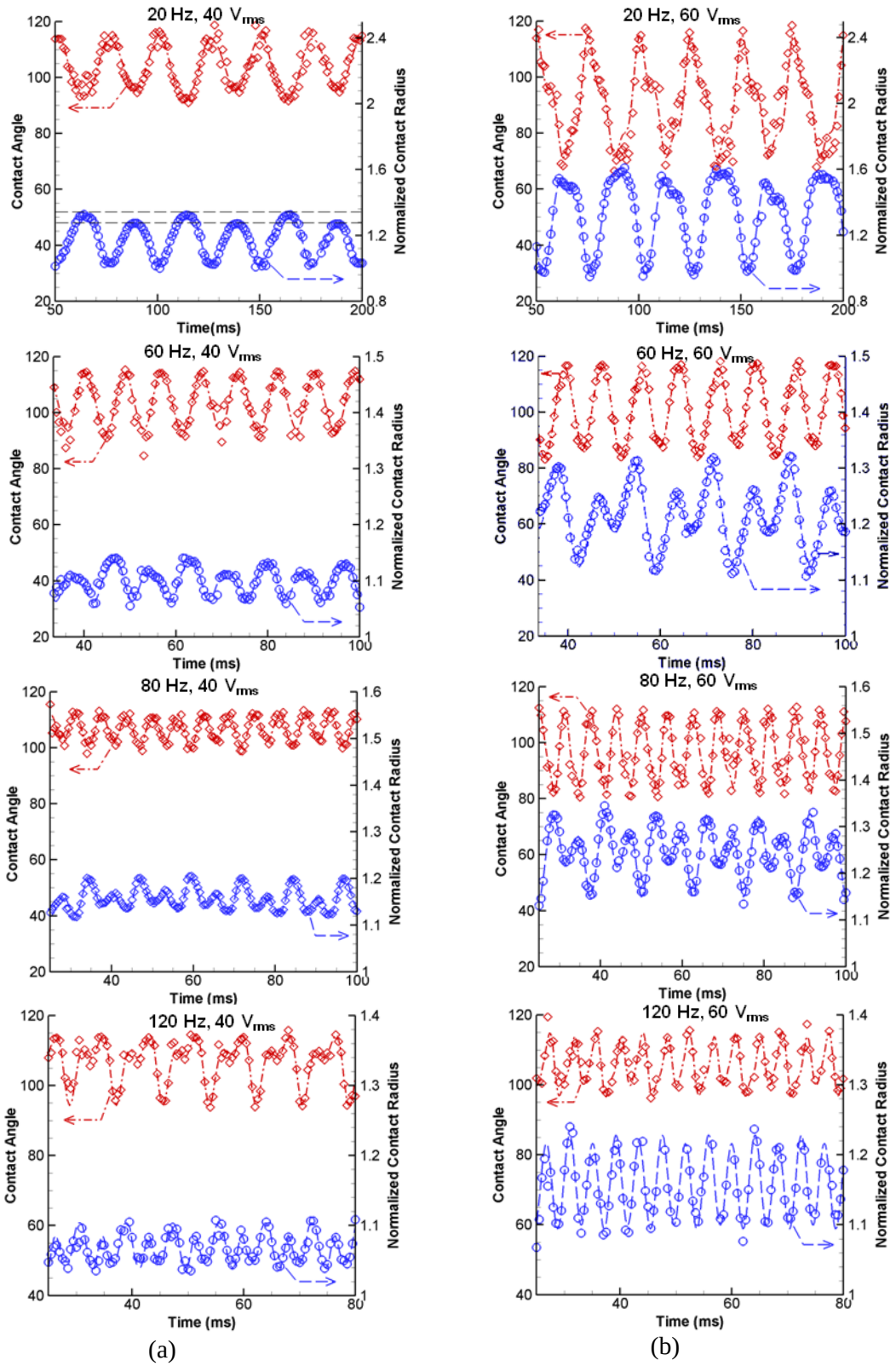

Figure 4. Variation of contact angles and contact radii for actuation frequencies of 20, 60, 80 and 120 Hz at (a) 40 V_{rms}, and (b) 60 V_{rms}.

3.2.2 Sub-harmonic oscillation

An interesting feature seen in the droplet oscillation (Figure 4) is the sub-harmonic behavior of the droplet contact radius; i.e., the maximum contact radii in successive droplet spreading cycles oscillate between two values. For example, at 40 V_{rms} and 20 Hz, the two values of the maximum contact radii are 1.3 and 1.24 as highlighted in Figure 4. The relative difference between these pairs of maximum contact radii increases as the actuation is AC frequency increased at the same actuation voltage. It is also observed that this behavior is not as pronounced in the contact radius variation at 40 V_{rms} and low frequencies of 20 Hz; however, at 40 V_{rms} with 80 Hz and 120 Hz, the contact radii do clearly exhibit such sub-harmonic behavior. Such behavior was also noted by Sen *et al*.[16] for one frequency, but was not explored in detail. Ko et. al.[31] observed the primary response of the droplet at the actuation frequency, i.e., at half the frequency of the applied electrical force during electrowetting driven oscillations of bubble. However such a droplet response has not been fully explained.

A Fast Fourier transform is performed on the raw data for contact angle and contact radius corresponding to the cases in Figure 4. The results are plotted in Figure 5 in order to capture the frequency response of the droplet oscillation under electrical actuation. The quality of the FFT plots is influenced by the finite number of data points used in the analysis. An integer number of oscillations are considered during the analysis, and random chopping off of the response data is avoided. All contact angles and radii have a maximum response at the frequency corresponding to that of the electrical force acting on the droplet, which is twice the applied actuation frequency (i.e, $2f_v$ where f_v is the actuation frequency). However, a significant response is also seen at the frequency (f_v) of the imposed signal in most cases. A super-harmonic response (less dominant than the sub-harmonic component) is observed in cases with high actuation voltage; the droplet response corresponding to 5 Hz and 60 V_{rms} demonstrates a stronger super-harmonic than 40 V_{rms}. At higher frequencies, the super-harmonic oscillation is suppressed. The ratios of the harmonic and the sub-harmonic responses for all cases are listed in Table 1 which clearly shows that the sub-harmonic response at the actuation frequency f_v increases with frequency and actuation voltage and is stronger in the contact radii traces as compared to the contact angle traces. Table 1 also includes the ratio of frequency responses corresponding to actuation at 5 Hz, 80 V_{rms} and 80 Hz, 80 V_{rms} which are not shown in Figure 4 and Figure 5 to avoid cluttering of the data points.

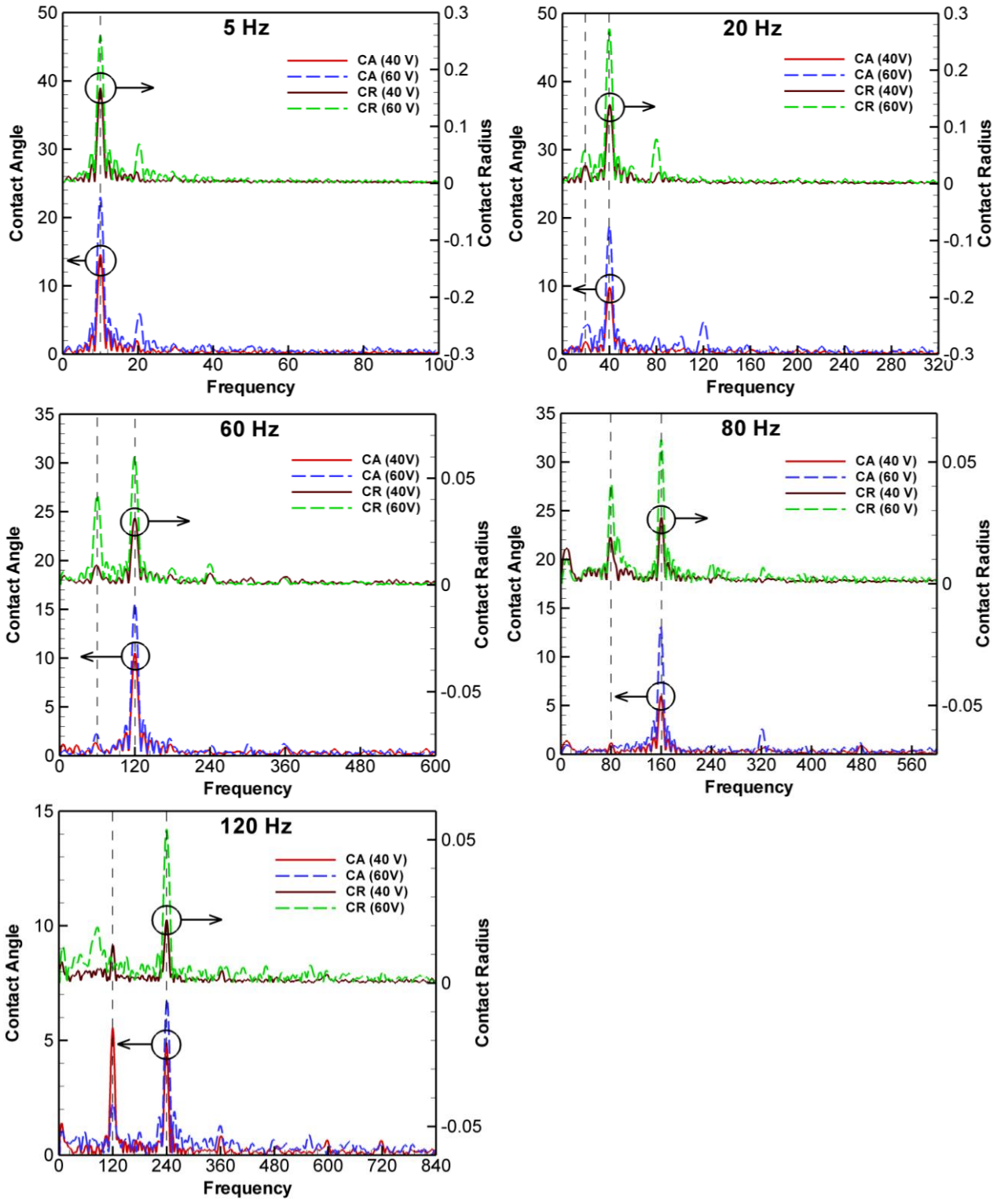

Figure 5. Fast fourier transforms for droplet response corresponding to AC frequencies of 5, 20, 60, 80, 120 Hz at applied voltages of 40 V_{rms} and 60 V_{rms}.

Table 1. Droplet response at forcing and sub-harmonic frequencies.

Frequency (Hz)	Applied Voltage (V_{rms})	Ratio of frequency response of CR at sub-harmonic (f_v) and harmonic frequencies ($2f_v$)	Ratio of frequency response of CA at sub-harmonic (f_v) and harmonic frequencies ($2f_v$)
5	40	0.06	0.04
	60	0.05	0.04
	80	0.10	0.10
20	40	0.23	0.19
	60	0.22	0.22
60	40	0.29	0.11
	60	0.70	0.14
80	40	0.69	0.20
	60	0.69	0.05
	80	1.90	0.06
120	40	0.60	1.13

In order to investigate the reason for the sub-harmonic oscillation observed, experiments are carried out under the application of both positive as well as negative potential at the substrate to determine the dependence of the polarity of the substrate on the electrowetted contact angle. The dependence of contact angle on the polarity at the substrate during electrowetting is determined by the material of the dielectric, which in our experiments is silicon dioxide. The contact angle variations with respect to applied voltage for both the polarities almost overlap (Figure 6). The average contact angle once saturation is reached is 72.9° ± 1.5° with positive potential at the substrate, and 73.9° ± 1.2° with negative potential at the substrate, which are essentially identical. This polarity independence of contact angle with the substrate used in the experiments is in agreement with the work of Cho *et al*.[2] who also observed the polarity-independence of a silicon dioxide substrate coated with Teflon. Hence it is unlikely that the electrical force has a secondary component.

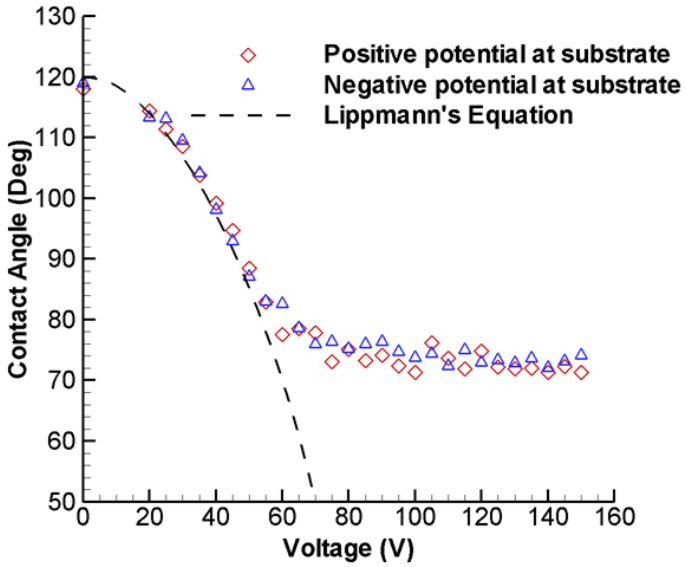

Figure 6. The contact angle of the droplet with the substrate maintained at positive and negative potentials.

When the electrical force acts at the TCL, it drives droplet oscillation and may excite several modes [32] depending upon the frequency of actuation. We present here an approach similar to that by Baret *et al*.[33] to determine the governing equation for droplet oscillation at the TCL and give a possible explanation for the sub-harmonic response of the droplet. The terms accounting for the modes (n) are neglected so as to give a simple expression for the transport equation. The Navier-Stokes equation representing balance of forces acting on the droplet can be written as

$$\frac{\partial u}{\partial t} + u \cdot \nabla u = \frac{1}{\rho}\left(\mu \nabla^2 u - \nabla p + f_e - \frac{F_f}{\forall} \right) \tag{2}$$

where $\forall$ is the droplet volume, f_e the electrical body force density and F_f the contact line friction. For water, the viscous dissipation can be neglected in comparison to the other forces acting during electrowetting [33]. For small oscillation, i.e., when the displacement of the contact line (x) is very small compared to the initial droplet radius ($x << R_c$), the non-linear convection term can be neglected [33]. The pressure gradient across the drop (∇p) can be approximated as $\nabla p = -\frac{\gamma}{R_c^{\,2}}\left(1 - \frac{2x}{R_c}\right)$. With an assumption that significant voltage drop occurs across the dielectric layer, the negative derivative of the stored energy (E) gives the electric force (F_e) acting on the droplet:

$$E = \frac{\varepsilon_0 \varepsilon_r A(r) V^2}{2d} \tag{3}$$

$$F_e = -\frac{dE}{dr} = -k' r (1 - \cos(2\omega t)) \tag{4}$$

where r is the contact radius $(r = R_c + x)$, $A(r)$ is the instantaneous interfacial area, $V = U\sin(\omega t)$ is the applied voltage; U is the amplitude of applied voltage, and $k' = \frac{\varepsilon_0 \varepsilon_r \pi}{2d} U^2$; the contact line friction is proportional to the velocity of the contact line [27,30] ($F_f = \xi \dot{x}(2\pi r)$), where ξ is the contact line friction coefficient.

Assuming that a constant mass, m is involved in the oscillation of the droplet, the final simplified expression for the droplet oscillation at the contact line, i.e., at $\theta = \pi/2$ takes the form:

$$\ddot{x} + \left(\frac{2\pi\xi}{m}(x + R_c)\right)\dot{x} + \left(\frac{2\gamma}{\rho R_c^3} - \frac{k'}{m}(1 - \cos(2\omega t))\right)x = \frac{k'}{m}\left(1 - \cos(2\omega t)\right)R_c + \frac{\gamma}{\rho R_c^2} \qquad (5)$$

As is obvious from Equation 5, the force acting on the TCL is parametric, i.e., it is a time-dependent force which also depends upon the magnitude of displacement (x).

This governing equation (Equation 5) is in the form of a parametrically excited and nonlinearly damped nonlinear equation [34]. The damping force, which is contact line friction in this case, as well as the forcing term are dependent on the instantaneous displacement of the contact line with respect to the initial contact radius. Depending upon the forcing amplitude (a function of the applied voltage), the governing equation is expected to have a sub-harmonic frequency as a solution together with the response at the forcing frequency (which is twice the frequency of the periodic input applied) in a particular range of frequency. The most convincing explanation for the sub-harmonic response of the droplet with periodic actuation at certain frequencies (> 20 Hz) is the Faraday instability [35], which is a characteristic outcome of the parametric excitation at the contact line. In the modified Pellat's experiment by Wang and Jones [30], a vigorous side-to-side sloshing motion of the liquid surface was observed when an electrical signal with frequency < 200 Hz was used to actuate the liquid (DI water) column. This phenomenon might be attributed to the parametric nature of the electrical force. Sub-harmonic oscillations have been studied in liquid droplets when a vertical oscillation is provided [36] and also in the case of magnetic actuation [37]. The important implication of this finding is that this phenomenon must be considered in droplet dynamics models for unsteady electrowetting-driven actuation.

3.2.2 Droplet oscillation regimes

The droplet contact line motion is significantly influenced by the frequency of actuation and the modes of oscillation as discussed in the previous section. In this section we determine the resonant frequencies of the droplet using Lamb's expression [38] and compare the values against the experimentally observed resonant frequencies, and determine the length scale appropriate for the determination of the same. The frequency regimes for in-phase and out-of-phase behavior of the droplet contact radius and contact angle are reported.

The bulk of the liquid can be treated as inviscid due to the low kinematic viscosity of 10^{-6} m^2/s of water. The natural oscillation of an inviscid liquid droplet in a gaseous medium has been well studied in the literature and the resonant frequency for the n^{th} mode oscillation is given by Lamb's expression [38] given by

$$f = \frac{1}{2\pi}\left[n(n-1)(n+2)\frac{\gamma}{\rho l^3} \right]^{1/2} \quad (6)$$

where ρ is the liquid density and l the characteristic droplet length. The characteristic droplet length for a droplet resting on a solid surface is not well-defined and hence, three lengths are considered: the droplet contact radius (R_c), the initial droplet radius before actuation (R_o), and the initial droplet height (h). For a droplet of volume 5 μl, using droplet contact angle as 120°, R_c = 0.9722 mm, R_o = 1.123 mm and h = 1.68 mm. All the length scales used are calculated using the spherical cap assumption of the droplet. Resonance occurs when the frequency of the electrical force (which is twice the frequency of the applied signal) matches the natural frequency of the droplet. The resonant frequencies for a 5 μl water droplet corresponding to these characteristic lengths are given in Table 2.

Table 2. Natural frequencies for the n^{th} oscillation mode using Lamb's expression (all frequencies are in Hz).

Mode, n	$l = R_c$		$l = R_o$		$l = h$	
	Resonant frequency of the droplet (Hz)	Corresponding Frequency of the applied voltage (Hz)	Resonant frequency of the droplet (Hz)	Corresponding Frequency of the applied voltage (Hz)	Resonant frequency of the droplet (Hz)	Corresponding Frequency of the applied voltage (Hz)
2	126.0	63.0	101.6	50.8	55.3	*27.6*
3	244.0	122	196.7	98.3	107.0	53.5
4	378.0	189.0	304.7	152.3	165.8	*82.9*
5	527.1	263.6	424.8	212.4	231.2	115.6
6	690.2	345.1	556.2	278.1	302.8	*151.4*

Droplet oscillation at 60 V_{rms} and frequencies from 5 Hz to 200 Hz in steps of 5 Hz is documented in Figure 7 to show the distinct frequency regimes and the effect of resonance on droplet oscillation dynamics within each regime. The figure shows four quantities as function of the frequency of the applied signal: the maximum displacement in the contact radius (defined as difference between the maximum and minimum contact radii for a given applied frequency; the CR prior to actuation is not used as the reference since a lower minimum contact radius is observed at frequencies close to resonance); the maximum contact radius attained; the instantaneous contact angle observed at the time instant when the maximum displacement in the contact radius is attained; and the minimum contact angle corresponding to each frequency. The displacement of the contact radius was used to experimentally determine the resonance frequencies. Intuitively, the instant of maximum contact radius of the droplet should correspond to the minimum contact angle (and *vice versa*). This in-phase behavior of the CR and CA is observed, for example, when the frequency is between 5 and 30 Hz. At these low frequencies (5 - 20 Hz), the droplet oscillates quasi-statically in response to the sinusoidal signal; a spherical cap assumption can be made for the droplet shape during oscillation. During the initiation of droplet

motion, video recordings reveal that the bulk of the liquid droplet moves downwards, thereby increasing contact radius. The droplet oscillation increases drastically at 40 Hz. Interestingly, the oscillation is more prominent in the height of the droplet rather than the radius of the droplet although the main electrical force is concentrated at the TCL.

The non-overlapping plots of instantaneous CA corresponding to maximum CR and the minimum CA at certain frequencies indicate the phase lag between the contact line motion and the contact angle. For actuation frequencies between 40 Hz and 70 Hz, the contact radius and contact angle become out-of-phase with the droplet oscillating in its 2^{nd} mode (as shown in the droplet shape at 40 Hz in the inset in Figure 7). The arrows around the droplet photograph show the nodal points. This is in agreement with the results of Lai *et al.*[39] who also observed out-of-phase behavior between the applied voltage and the droplet motion at the droplet resonant frequencies. The droplet reverts to its in-phase behavior at a frequency of approximately 70 Hz. However, the contact line oscillation is much reduced at these frequencies. The magnitude of oscillation is at its minimum until the frequency of the AC signal is increased to a value of approximately 100 Hz, at which the contact line movement increases significantly and the droplet continues to oscillate with the contact angle being in-phase with the contact radius. Beyond 100 Hz, a prominent 4^{th} mode of oscillation is observed in the droplet (Figure 7). The droplet oscillation exhibits out-of-phase behavior beyond a frequency of 115 Hz until the 6^{th} mode of oscillation becomes dominant at frequencies higher than 180 Hz. Figure 7 shows the droplet oscillating in the 6^{th} mode of oscillation at a frequency of 190 Hz. The closest agreement between the experimentally obtained resonance frequencies and those predicted using Equation 6 is found when droplet height is selected as the characteristic length; this is consistent with the experimental observations of Kim [40].

An interesting correlation is seen between the contact angle and contact radius as a function of the frequency of AC actuation. After the droplet attains a resonance frequency, the CR and CA go out of phase; this continues till the next higher level of resonance frequency is dominant. The change in phase is accompanied by minimal contact line movement; the contact line is almost pinned during this time and the oscillation takes the form of varying contact angle. Whether the droplet oscillates in-phase or out-of-phase is a characteristic of the droplet that is directly related to the resonance phenomenon. The magnitude of oscillation and the phase angle between the CR and CA is also a result of the interaction between the different modes of oscillation of the droplet. Accordingly, droplets of different volumes will show in-phase or out-of-phase behavior corresponding to different values of actuation frequencies. Further study of the interaction between different modes during oscillation of a constrained droplet would help in understanding the detailed dynamics in terms of analytical determination of the exact magnitude of oscillation and corresponding contact angle.

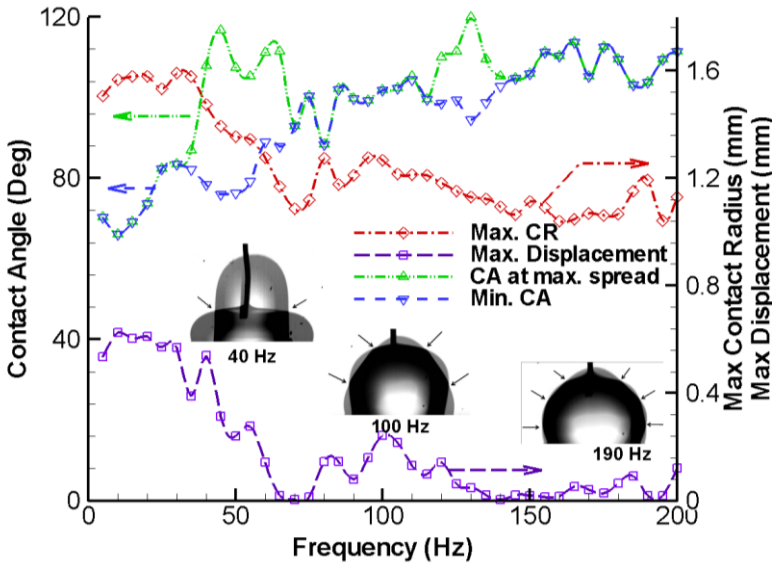

Figure 7. Droplet oscillation at 60 V_{rms} over a 5 Hz to 200 Hz frequency range. The instantaneous contact angle (green triangle) corresponding to the time instant of maximum contact radius (red diamond), the minimum contact angle (blue gradient) and the maximum displacement of the contact radius (purple square) are shown. The images shown as insets demonstrate distinct modes of droplet oscillation corresponding to three different frequencies (40 Hz, 100 Hz and 190 Hz)

4. Conclusion

The transient response of a droplet to step actuation has been experimentally demonstrated. The local oscillations induced in the droplet result in a finite delay in the droplet achieving its steady-state profile. The droplet takes approximately 9 ms for a 5 μl droplet to reach the maximum contact radius irrespective of the voltage applied. It is demonstrated that the characteristic time scale is dependent upon the radius, density and surface tension of the droplet and should be taken into account in designing practical systems that exploit electrowetting actuation.

A detailed experimental study of the droplet dynamics reveals the dependence of the contact angle and contact radius on the applied frequency and voltage of a periodic sinusoidal signal. The droplet follows the signal at low AC frequencies and the oscillations are mostly electrowetting-induced. At higher frequencies, distinct shape oscillation modes are induced which, along with resonance, determines the magnitude of oscillation and phase angle between contact angle and contact radius. The contact angle and contact radius show an alternating in-phase and out-of-phase behavior between successive resonant frequencies. The experimentally determined resonance frequencies are shown to be well estimated by Lamb's expression for natural frequency of a droplet when the height of the droplet is taken as the characteristic length scale in the prediction. Sub-harmonic oscillations of the droplet contact radius and contact angle during electrowetting are identified and are explained in terms of the parametrically excited nonlinear equation governing the droplet oscillation. These sub-harmonic oscillations are attributed to the nonlinear damping forces and the parametric excitation force acting on the droplet during electrowetting.

ACKNOWLEDGEMENT

The authors thank Prof. Anil K. Bajaj for his help with modeling of the droplet frequency response. Funding from the National Science Foundation for this work as a Fundamental Research Supplement to the Cooling Technologies Research Center, an Industry/Cooperative Research Center, is gratefully acknowledged.

REFERENCES

[1] Mugele F and Baret J C 2005 Electrowetting: from basics to applications *Journal of Physics: Condensed Matter* **17** R705

[2] Cho S K, Moon H and Kim C J 2003 Creating, transporting, cutting, and merging liquid droplets by electrowetting-based actuation for digital microfluidic circuits *Journal of Microelectromechanical Systems* **12** 70-80

[3] Pollack M G, Shenderov A D and Fair R B 2002 Electrowetting-based actuation of droplets for integrated microfluidics *Lab on a Chip* **2** 96-101

[4] Chatterjee D, Hetayothin B, Wheeler A R, King D J and Garrell R L 2006 Droplet-based microfluidics with nonaqueous solvents and solutions *Lab on a Chip* **6** 199-206

[5] Kumari N, Bahadur V and Garimella S V 2008 Electrical actuation of dielectric droplets *Journal of Micromechanics and Microengineering* **18** 085018

[6] Kumari N, Bahadur V and Garimella S V 2008 Electrical actuation of electrically conducting and insulating droplets using ac and dc voltages *Journal of Micromechanics and Microengineering* **18** 105015

[7] S. Kuiper S, and Hendriks B H W 2004 Variable-focus liquid lens for miniature cameras *Applied Physics Letters* **85** 1128

[8] Hayes R A and Feenstra B J 2003 Video-speed electronic paper based on electrowetting *Nature*, **425** 383-385

[9] D Herbertson D L, Evans C R, Shirtcliffe N J, McHale G and Newton M I 2006 Electrowetting on superhydrophobic SU-8 patterned surfaces *Sensors and Actuators A: Physical* **130** 189-193

[10] Bahadur V and Garimella S V 2007 Electrowetting-based control of static droplet states on rough surfaces *Langmuir* **23** 4918-4924

[11] Bahadur V and Garimella S V 2008 Electrowetting-based control of droplet transition and morphology on artificially microstructured surfaces *Langmuir* **24** 8338-8345

[12] Shapiro B, Moon H, Garrell R and Kim C 2003 Equilibrium behavior of sessile drops under surface tension, applied external fields, and material variations *Journal of applied physics* **93** 5794-5811

[13] Vallet M, Vallade M and Berge B 1999 Limiting phenomena for the spreading of water on polymer films by electrowetting *The European Physical Journal B - Condensed Matter and Complex Systems* **11** 583-591

[14] Roques-Carmes T, Hayes R A and Schlangen L J M 2004 A physical model describing the electro-optic behavior of switchable optical elements based on electrowetting *Journal of Applied Physics* **96** 6267

[15] Oh J M, Ko S H and Kang K H 2010 Analysis of electrowetting-driven spreading of a drop in air *Physics of Fluids* **22** 032002

[16] Sen P and Kim C 2009 Capillary Spreading Dynamics of Electrowetted Sessile Droplets in Air *Langmuir* **25** 4302-4305

[17] Cooney C G, Chen C Y, Emerling M R, Nadim A and Sterling J D 2006 "Electrowetting droplet microfluidics on a single planar surface *Microfluidics and Nanofluidics* **2** 435-446

[18] Kumar A, Pluntke M, Cross B, Baret J C and Mugele F 2006 Finite conductivity effects and apparent contact angle saturation in AC electrowetting *in Mater. Res. Soc. Symp. Proc* 0899-N06-01

[19] Jones T B, 2001 Liquid dielectrophoresis on the microscale *Journal of Electrostatics* **51** 290-299

[20] Berge B and Peseux J 2000 Variable focal lens controlled by an external voltage: an application of electrowetting *The European Physical Journal E: Soft Matter and Biological Physics* **3** 159-163

[21] Mugele F, Staicu A, Bakker R and van den Ende D 2011 Capillary Stokes drift: a new driving mechanism for mixing in AC-electrowetting *Lab on a Chip* **11** 2011-2016
[22] Paik P, Pamula V K and Fair R B 2003 Rapid droplet mixers for digital microfluidic systems *Lab on a Chip* **3** 253-259
[23] Miraghaie R, Sterling J D and Nadim A 2006 Shape Oscillation and Internal Mixing in Sessile Liquid Drops using ElectroWetting-On-Dielectric (EWOD) *Technical Proceedings of the 2006 NSTI Nanotechnology Conference and Trade Show* 610–613
[24] Mugele F, Baret J C and Steinhauser D 2009 Microfluidic mixing through electrowetting-induced droplet oscillations *Applied Physics Letters* **88** 204106
[25] Ko S H, Lee H and Kang K H 2008 Hydrodynamic flows in electrowetting *Langmuir* **24** 1094-1101
[26] MATLAB, 2007 Reference Manual (Natick MA: The Mathworks Inc.)
[27] Ren H, Fair R B, Pollack M G and Shaughnessy E J 2002 Dynamics of electro-wetting droplet transport *Sensors and Actuators B: Chemical* **87** 201-206
[28] Annapragada S R, Dash S, Garimella S V and Murthy J Y 2011 Dynamics of Droplet Motion under Electrowetting Actuation *Langmuir* **27** 8198-8204
[28] Richard D, Clanet C and Quere D 2002 Surface phenomena: Contact time of a bouncing drop Contact time of a bouncing drop *Nature*, **417**, 811
[30] Wang K L and Jones T B 2005 Electrowetting dynamics of microfluidic actuation *Langmuir* **21** 4211-4217
[31] Ko S H, Lee S J and Kang K H 2009 A synthetic jet produced by electrowetting-driven bubble oscillations in aqueous solution *Applied Physics Letters* **94** 194102
[32] Oh J M, Ko S H and Kang K H 2008 Shape Oscillation of a Drop in ac Electrowetting *Langmuir* **24** 8379-8386
[33] Baret J C, Decre M M and Mugele F 2007 Self-excited drop oscillations in electrowetting *Langmuir* **23** 5173-5179
[34] Jordan D W and Smith P 1977 Nonlinear ordinary differential equations Clarendon Press Oxford
[35] Miles J and Henderson D 1990 Parametrically forced surface waves *Annual Review of Fluid Mechanics* **22** 143-165
[36] Noblin X, Buguin A and Brochard-Wyart F 2009 Vibrations of sessile drops *The European Physical Journal-Special Topics* **166** 7-10
[37] Malouin Jr B A, Koratkar N A, Hirsa A H and Wang Z 2010 Directed rebounding of droplets by microscale surface roughness gradients *Applied Physics Letters* **96** 234103
[38] Lamb H 1932 Hydrodynamics 6th ed Cambridge University Press: Cambridge UK
[39] Lai M F, Lee C P, Liao C N and Wei Z H 2009 Oscillation spectrums and beat phenomenon of a water droplet driven by electrowetting *Applied Physics Letters* **94** 154102
[40] H. Y. Kim 2004 Drop fall-off from vibrating ceiling *Physics of Fluids* **16** 474-477